A Current Chopper-Assisted Magnetic Field-Based Backscatter Communication Method With WPT Overcoming Ultralow Coupling Coefficients

Ryota Fukugasako, Hisafumi Asaue, Tomoki Shiotani, Masanori Hashimoto, *Senior Member, IEEE*, and Ryo Shirai, *Member, IEEE*

***Abstract*—This article proposes a magnetic-field-based backscatter communication method that enables ultralow-power wireless communication. In this approach, a client node extracts energy from a magnetic field for wireless power transfer (WPT) and backscatters it while embedding information. The client node modulates the magnetic field for WPT by chopper-controlling the current in its power-receiver coil, eliminating the need for power-hungry oscillators. As a result, communication is achieved using only the energy required to drive the gate of a MOSFET, leading to significant power savings. Experimental validation with a prototyped system demonstrated a receivable power of 1.52 mW, a 38% increase over existing chopper-based methods, at a distance of 50 cm. In addition, simulations using a TSMC 180-nm process revealed that communication energy can be reduced to 0.36 pJ/bit, achieving more than a 90% reduction compared with conventional approaches. These results confirm that the proposed method greatly enhances energy efficiency, making it suitable for submeter-range, low-power wireless communication in embedded sensor applications, such as infrastructure monitoring.**

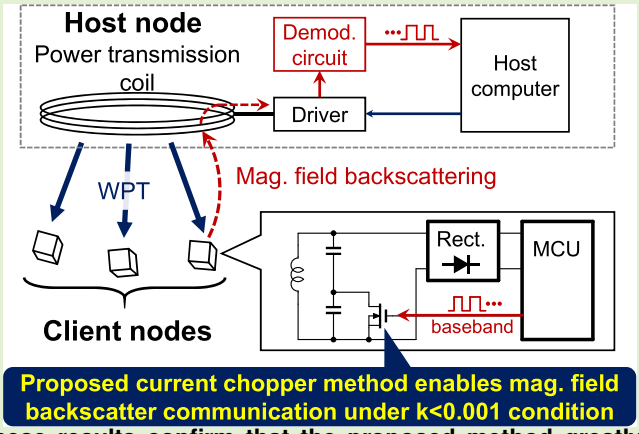

***Index Terms*—Backscatter communication, current chopper, inductive coupling, wireless communication, wireless power transfer (WPT).**

I. Introduction

REINFORCED concrete (RC) has been used as a common bridge deck material for over a century due to its low cost, wide availability, and versatility in construction. As cracking are well-developed for RC structures due to aging, inspections shall be regularly carried out to promote preventive maintenance resulting in reduction of structural risks and maintenance cost.

Current methods, such as visual inspections and tapping tests, are labor-intensive and require skilled specialists, increasing the overall cost. A declining birthrate and resultant increase in aging population have reduced the number of skilled workers and lowered tax revenues, implying the necessity to develop autonomous inspection technique to address those challenges as not to disrupt logistics and economic activities with road infrastructures [1], [2].

To address these challenges, we propose and are developing a system that uses embedded sensors in RC during construction to detect cracks efficiently. Fig. 1 illustrates an overview of the proposed detection framework under development. An inspection vehicle induces vibrations in the RC, and the embedded sensors detect these vibrations to estimate crack locations. This system requires four key components: 1) crack detection by embedded sensors; 2) localization of embedded sensors, 3) wireless power transfer (WPT) to the

Received 6 March 2025; revised 24 March 2025; accepted 24 March 2025. Date of publication 1 April 2025; date of current version 15 May 2025. This work was supported by JSPS KAKENHI under Grant JP21K21284 and Grant JP22K17867. The associate editor coordinating the review of this article and approving it for publication was Prof. Huang Chen Lee. *(Corresponding author: Ryo Shirai.)*

Ryota Fukugasako, Masanori Hashimoto, and Ryo Shirai are with the Department of Informatics, Kyoto University, Kyoto 606-8501, Japan (e-mail: fukugasako.ryota.38w@st.kyoto-u.ac.jp; hashimoto@i.kyoto-u.ac.jp; shirai@i.kyoto-u.ac.jp).

Hisafumi Asaue and Tomoki Shiotani are with the Office of Institutional Advancement and Communications, Kyoto University, Kyoto 606-8501, Japan (e-mail: asaue.hisafumi.7a@kyoto-u.ac.jp; shiotani.tomoki.2v@kyoto-u.jp).

Digital Object Identifier 10.1109/JSEN.2025.3555072

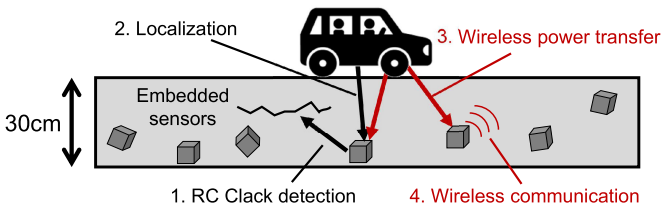

Fig. 1. Overview of the RC crack detection system.

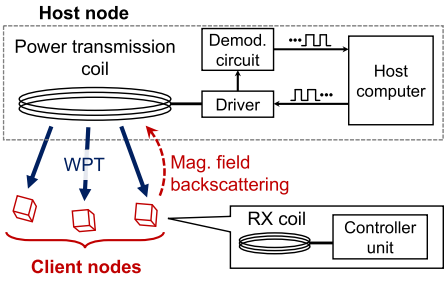

Fig. 2. Overview of the proposed system.

sensors; and 4) wireless communication from the sensors to the vehicle. Among these, components 1) and 2) have been widely studied in research that is directly applicable. For crack detection, acoustic emission-based methods have been extensively studied [3], [4], [5] and can be adapted for this research. To localize the sensors, the dc magnetic-field-based approach proposed in [6], [7], and [8] achieves localization accuracy of less than 1 cm. Finally, magnetic-field-based WPT methods [9], [10], [11], [12], [13] provide power wirelessly over several tens of centimeters.

Wireless communication from the sensors, the remaining key component, is required to transmit the detected crack locations to the inspection vehicle. For this wireless communication, available options include Bluetooth Low Energy (BLE) [14], [15], [16] and Wi-Fi [17], [18], [19], both of which use oscillators to generate carrier waves. However, oscillators consume significant power during start-up, requiring energy storage components such as supercapacitors or batteries. These components, however, are unsuitable due to their vulnerability to thermal degradation during concrete casting [20], [21], [22].

To overcome this limitation, backscatter communication, which transmits information by modulating the reflection of ambient RF signals, has been investigated [23], [24], [25], [26], [27]. Although backscatter communication is energy-efficient and does not require energy storage, this method requires large antennas for impedance matching, making it impractical for small sensors.

In pursuit of antenna-free communication, magnetic-field-based wireless communication has been explored [28], [29], [30], [31], [32], [33], [34]. This method relies on inductive coupling between coils implemented in the transmitter and receiver. However, generating a magnetic field strong enough for wireless communication requires a high current, resulting in significant power consumption. To reduce the current consumption for generating magnetic field, magnetic-field-based backscatter communication is widely used as a low-power wireless communication method in which a client node transmits data by modulating its interaction with the alternating magnetic field generated by a host node. In this system, the host node is responsible for both WPT and communication, while the client node remains passive, thereby eliminating the need for active power-hungry components. The client node receives power from the host node's magnetic field and transmits data by altering its coil impedance, a technique known as "load modulation." This method has been studied and is already used in practical applications such as near-field communication (NFC) and radio frequency identification (RFID) [35].

Conventional magnetic field-based backscatter communication relies on load modulation, where the impedance of the client coil is switched to induce detectable fluctuations in the current of the host coil. However, when the coupling coefficient is extremely low, these fluctuations become too small to be detected, making conventional methods impractical for tens-of-centimeter-range communication required for our RC crack detection application [36].

To address this limitation, this article proposes a magnetic-field-based backscatter communication method that enhances communication reliability even under ultralow coupling conditions. Unlike conventional methods, the proposed system uses current chopper control to modulate the induced current in the client coil at its peak, optimizing the interaction with the ac magnetic field for WPT. This technique significantly improves the detectability of the backscattered signal, enabling communication even at extremely low coupling coefficients. The proposed method is well-suited for integration with WPT in small-volume sensors, providing reliable wireless communication with minimal power consumption.

II. Proposed Method

Fig. 2 shows an overview of the proposed magnetic-field-based backscatter communication system. The host node on the inspection vehicle generates an ac magnetic field to wirelessly power the client nodes, which are sensors embedded in RC structures. The client nodes then transmit information using the proposed backscatter communication method.

A. Client Node Design

Fig. 3 illustrates the circuit structure of the proposed client node. The client node consists of an LC tank (C_{c1}, C_{c2}, and L_c), a full-wave rectifier, energy storage capacitors (C_{st1} and C_{st2}), a load circuit (modeled as R_L), a MOSFET switch (Q1), and a controller. During WPT, the LC tank captures energy from the ac magnetic field generated by the host node. The full-wave rectifier converts the induced ac voltage at the LC tank into dc, which is stored in C_{st1} and C_{st2}. The load circuit represents the sensor's power consumption. For the proposed backscatter communication, the controller adjusts the gate voltage of Q1 to change the resonance frequency of the client node. This frequency adjustment alters the current flowing through the LC tank, affecting its interaction with the power transmission coil in the host node. As the client node modulates this interaction through the gate voltage, the host node perceives the modulation, enabling data transmission.

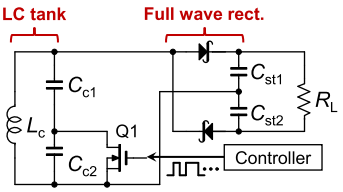

Fig. 3. Circuit diagram of the proposed client node.

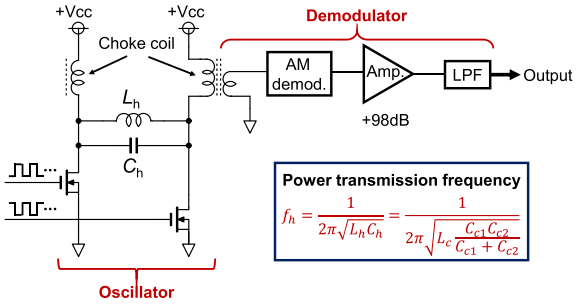

Fig. 4. Structure of the proposed host node.

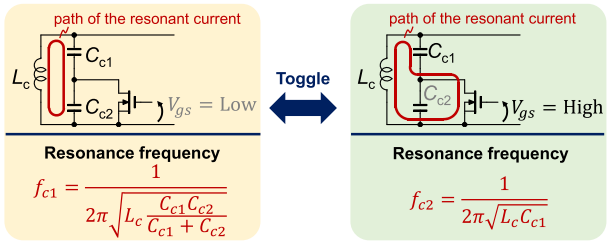

Fig. 5. Switching of resonance frequency in the proposed client node.

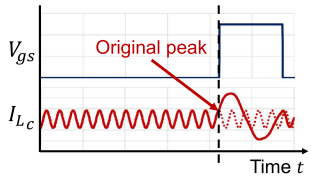

Fig. 6. Expected behavior of the proposed client node.

B. Host Node Design

Fig. 4 shows the circuit structure of the host node, which comprises an oscillator for power transmission and a demodulator for signal extraction. The oscillator includes a dc power source, an LC resonator (C_h and L_h), MOSFETs, and choke coils. The dc power source supplies current through the choke coils. The two MOSFETs are controlled to achieve zero-voltage switching (ZVS) to minimize switching losses. Reducing switching losses allows a large resonant current to flow through the power transmission coil (L_h), thereby generating a strong ac magnetic field for WPT. The demodulator consists of a coupling coil, an AM demodulator, an amplifier, and a low-pass filter (LPF). The coupling coil is magnetically coupled with the choke coil in the oscillator circuit to extract variations in the magnetic field caused by the client node for backscatter communication. The detailed signal processing method will be explained in Section II-C.

C. Proposed Backscatter Communication

In the proposed backscatter communication, the client node transmits data to the host node by modulating the ac magnetic field used for WPT. This modulation is achieved by adjusting the resonant frequency of the client node through the control of the gate voltage of a MOSFET. Fig. 5 illustrates the resonance frequencies of the client node under different states of switch Q1. When $V_{\rm gs}$ is set to a low voltage, Q1 acts as an open switch, and the client node resonates at the frequency of f_{c1}, which matches the power transmission frequency f_h, as shown in Fig. 4. When $V_{\rm gs}$ is set to a high voltage, Q1 shorts C_{c2}, shifting the resonance frequency to f_{c2}. Consequently, the current I_{L_c} flowing through L_c decreases since f_{c2} significantly differs from the power transmission frequency f_h.

During WPT operation, $V_{\rm gs}$ is set to a low voltage and Q1 remains open, allowing the client node's resonance frequency to match f_h. This enables sufficient current I_{L_c} to flow through L_c, which is rectified by the full-wave rectifier to charge the capacitors. Even if the energy stored in the capacitors depletes, Q1 defaults to an open state, ensuring continuous power supply from the host node to the client node. This feature also allows sensors to have cold-start capability.

In the proposed backscatter communication, the client node modulates the magnetic field generated by the host node by chopping the current I_{L_c}. This is achieved by changing the voltage applied to the gate of Q1, which alters the interaction between the LC tank and the ac magnetic field for WPT. As a result, variations in the magnetic field cause fluctuations in the current flowing through the host coil. By monitoring these fluctuations, the host node can detect the switching state of Q1 and decode the transmitted data. Fig. 6 shows the waveform of I_{L_c} during the switching operation of Q1. Initially, $V_{\rm gs}$ is low, and an ac current with a frequency of f_h flows through L_c. When I_{L_c} reaches its peak and is detected by the microcontroller unit (MCU), $V_{\rm gs}$ is immediately switched to a high. This shift in resonance frequency gradually reduces the amplitude of I_{L_c}. As a result, the frequency of I_{L_c} drops significantly, generating a low-frequency component superimposed on the ac magnetic field for WPT. The host node extracts the signal applied to the gate of Q1 by detecting this low-frequency component from the superimposed magnetic field. Notably, the proposed method is well-suited for sensors without energy storage, as it requires power only for MOSFET gate control, enabling a cold start capability.

The demodulation process at the host node uses the variations in the current flowing through the power transmission coil. These variations can be detected by monitoring the output current of the power source. In addition, the low-pass characteristics of the choke coil facilitate the detection of low-frequency baseband signals. Signals are extracted from the coil coupled with the choke coil and processed through an AM demodulator, amplifier, and LPF. The key mechanism enabling AM demodulation is as follows: When the client node switches its MOSFET, it alters the resonance condition of its LC tank circuit, thereby changing the amplitude of the current flowing through the client coil. This amplitude variation affects the degree of interference with the ac magnetic field generated by the host node, modulating the local magnetic field strength.

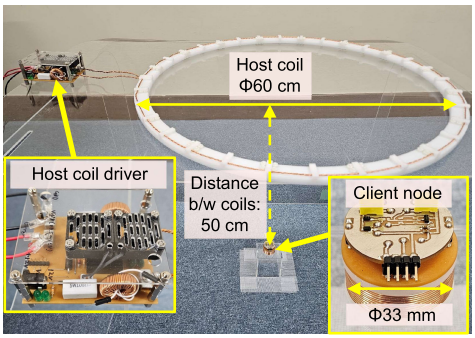

Fig. 7. Prototyped host node and client node.

Consequently, the current amplitude in the host coil varies over time, creating an envelope that follows the switching pattern of the MOSFET. Since this envelope carries the transmitted data, AM demodulation is used to extract the transmitted signal.

III. Evaluation

This section presents the experimental evaluation of the proposed magnetic-field-based backscatter communication system. Both WPT and backscatter communication performances are evaluated because the proposed communication method relies on the magnetic field used for WPT.

A. Setup

This section describes the experimental setup. Hardware prototypes of the host node and client node were implemented based on the structures shown in Figs. 3 and 4. Fig. 7 shows the prototyped devices and experimental setup.

For the client node, L_c has a diameter of 33 mm and comprises 26 turns of copper wire with a thickness of 0.8 mm. C_{st1} and C_{st2} are implemented using 0.1-μF capacitors. IRFML8244 is used for MOSFET Q1. The sensor device for RC crack detection is assumed to have power consumption characteristics similar to those of a microcontroller (PIC12LF 1822), and an elastic wave sensor (ADXL1001), consuming approximately 0.9 mW at 3 V. This power consumption is equivalent to a load resistance of approximately 10 kΩ, which is used as the value of R_L in the experiment.

For the host node, L_h has a diameter of 600 mm and consists of a single turn. The power transmission frequency f_h is set to 318 kHz to match the resonance frequency of the LC resonator in the host node. The AM demodulation stage is implemented using an envelope detector circuit with a Schottky barrier diode (BAT54). The BAT54 diode is selected due to its low forward voltage drop and fast switching characteristics, which enhance the detection efficiency for weak amplitude-modulated signals. The amplification stage in the demodulator section in Fig. 4 consists of three cascaded noninverting amplifier circuits, each providing a voltage gain of 26.4 dB, and one additional noninverting amplifier with a voltage gain of 20.8 dB. These amplifiers are implemented using LT1013 operational amplifiers, which offer low offset voltage and low input bias current, making them suitable for precise signal amplification. A second-order Sallen–Key LPF is used to extract the baseband signal while attenuating the power transmission signal. Since their frequencies are relatively close, the Sallen–Key topology, with its steep cutoff characteristics, ensures effective separation and stable frequency response. The Vcc node labeled in Fig. 4 is connected to the power source.

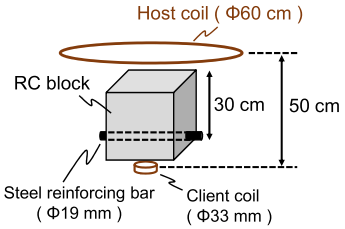

Fig. 8. Experimental setup incorporating an RC block.

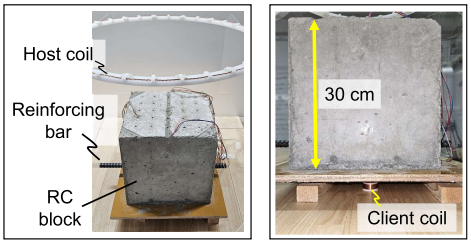

Fig. 9. Photograph of the experimental setup with an RC block: (a) overall view and (b) side view.

Fig. 7 shows the experimental setup. The client and host coils are positioned facing each other at a distance of 50 cm, representing the maximum communication range. This distance is based on a typical road thickness of approximately 30 cm and a 20-cm gap between the inspection vehicle's floor and the road surface, simulating a realistic deployment scenario. While Fig. 7 depicts the setup without RC, we also conducted experiments using an actual RC block, as shown in Figs. 8 and 9. Fig. 8 presents the experimental setup incorporating the RC block, while Fig. 9 provides a photograph of the installed RC block, host coil, and client coil. As illustrated in Fig. 9, multiple cables are protruding from the RC block because additional wired sensors were embedded for separate experiments, which are not related to this study. In the following experiments, the output voltage is evaluated using an oscilloscope (GDS-2204A).

B. Evaluation of Coupling Coefficient

We first evaluate the coupling coefficient between the host and client coil, as the proposed method relies on inductive coupling. The evaluation was conducted in two setups: without an RC block, as shown in Fig. 7, and with an RC block, as depicted in Fig. 8. To measure the coupling coefficient, we measured the voltage across both the host (L_h) and client (L_c) coils. The coupling coefficient k is related to L_h, L_c, and the mutual inductance M as follows: $M = k\sqrt{L_h L_c}$. From the equivalent circuit shown in Fig. 10, the voltage V_2 satisfies

$$V_2 = \frac{j\omega M V_1}{j\omega(L_h - M) + j\omega M} = \frac{M}{L_h} V_1 = k\sqrt{\frac{L_c}{L_h}} V_1. \quad (1)$$

Thus, k is obtained from the measured inductances L_h and L_c, and the voltages V_1 and V_2 as

$$k = \frac{V_2}{V_1}\sqrt{\frac{L_h}{L_c}}. \quad (2)$$

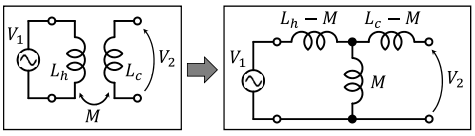

Fig. 10. Equivalent circuit of magnetically coupled coils L_1 and L_2.

The measured coupling coefficient without the RC block was 5.93×10^{-4}, whereas with the RC block, it was 5.75×10^{-4}. These results indicate that while the presence of the RC block slightly degrades the coupling coefficient, the impact remains minimal. Therefore, the subsequent evaluations are conducted in the setup without the RC block, which is depicted in Fig. 7.

C. Evaluation of WPT Performance

We next evaluate the WPT performance of the proposed system. The client node must receive sufficient power to operate the sensor device and maintain gate voltage control for backscattering. The evaluation was conducted under the condition where $V_{\mathrm{gs}} = 0$. The results showed that the client node received 1.52 mW of power at a distance of 50 cm, sufficient to operate the sensor device consuming 0.9 mW. The proposed system can receive power even when the energy in the device is completely depleted and the gate voltage cannot be applied, thereby providing a cold-start capability. This contrasts with the method described in [10], which fails to supply power when the device's internal energy is depleted.

D. Evaluation of Backscatter Communication Performance

We finally evaluate backscatter communication by applying a 0.89-kHz baseband pulse to the gate of MOSFET Q1 at the client node. Fig. 11 shows the waveforms of V_{gs} at the client node and the demodulator output at the host node. The results show that the demodulator output changes in response to V_{gs}. This indicates that the host node can detect the switching state of Q1 by observing the demodulator output. We thus confirm that the proposed magnetic-field-based backscatter communication is feasible and satisfies the communication distance requirement of the crack detection system.

To further evaluate the communication performance of the proposed system, we measured the signal-to-noise ratio (SNR) using the hardware prototype. During the experiment, the signal at the host node fluctuated continuously, causing the SNR of the received signal to vary over time. The client node transmits data in the form of pulses, as shown in Fig. 11. SNR was calculated as $\mathrm{SNR} = 20\log(V_{\mathrm{sig}}/V_{\mathrm{nf}})$, where $V_{\mathbf{sig}}$ is the detected pulse amplitude and V_{nf} is the amplitude of background noise, which was 7.6 Vpp as shown in Fig. 11. The measurement results showed that the maximum and minimum SNR values were 5.8 and 3.8 dB, respectively.

Furthermore, we conducted bit error rate (BER) measurements using the prototype system. In the experiment, the client node transmitted 957-bit pulses to the host node. Out of these, 883 bits were received with an SNR exceeding 3.5 dB, which is the minimum threshold for successful demodulation with the prototyped receiver. From these results, the calculated BER of the prototype system was 7.73×10^{-2}.

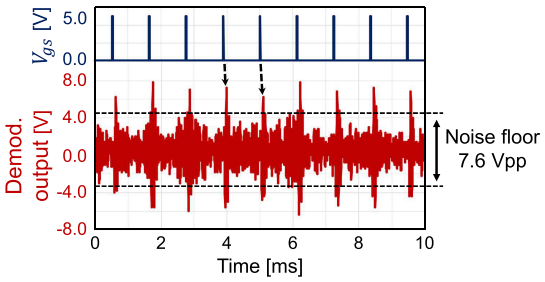

Fig. 11. Transmitted and received signals.

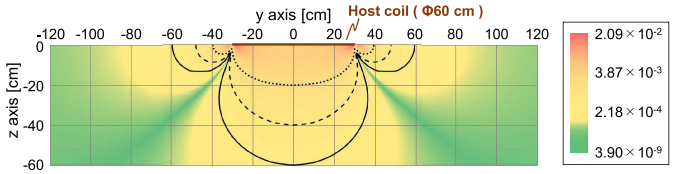

Fig. 12. Heatmap and contour lines of the coupling coefficient distribution between the host and client coils.

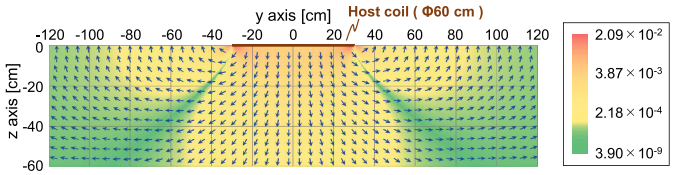

Fig. 13. Magnetic field vectors at various positions around the host coil.

Here, it should be noted that the measured SNR and BER values were obtained using a preliminary receiver design with a basic demodulation circuit. There remains significant room for improvement in reception performance through the design of appropriate amplifiers, demodulation circuits, and filtering circuits. Future work will focus on optimizing these components to further enhance the communication reliability of the proposed system.

IV. Discussion

A. Coupling Coefficient Distribution and Dynamic Scenario Feasibility

To evaluate the feasibility of the proposed backscatter communication in dynamic scenarios, we numerically analyzed the coupling coefficient distribution around the coils, as shown in Figs. 12 and 13. As described in Section III-B, the coupling coefficient k satisfies the following relationship: $k = M/\sqrt{L_h L_c}$. The mutual inductance M is determined by the total magnetic flux passing through L_c when a unit current is applied to L_h. Hence, the coupling coefficient can be numerically computed using the following equation:

$$k = \frac{1}{\sqrt{L_h L_c}} \int_{S_c} \mathbf{B}_p \cdot \mathbf{e}_{L_c} dS \tag{3}$$

where S_c represents the cross-sectional area enclosed by L_c, and $\mathbf{e}_{L_c}$ is the unit vector aligned with the axis of L_c. $\mathbf{B}_p$ represents the magnetic flux density at the point p in the area enclosed by L_c and is calculated using the Biot–Savart law.

Fig. 12 presents a heatmap and contour lines representing the spatial distribution of the coupling coefficient. For instance, the contour lines at $z = 60$ [cm] indicate that the coupling

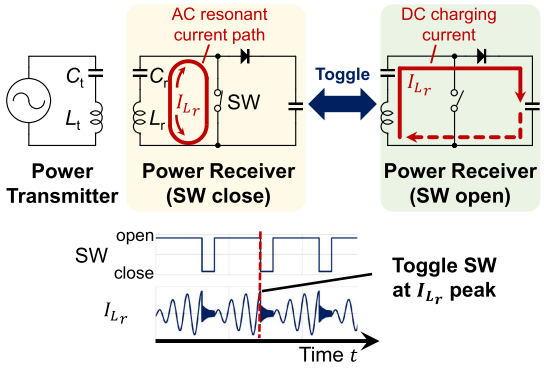

Fig. 14. Behavior of the client node in current chopper-based WPT [10].

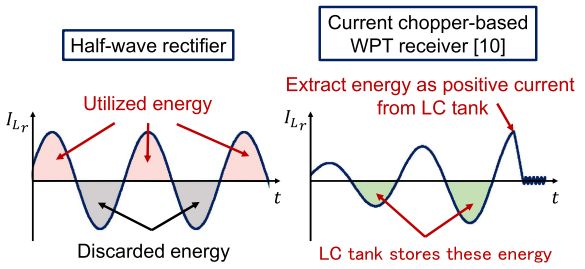

Fig. 15. Current flow through receiver coil in each WPT method.

coefficient remains relatively stable over a broad lateral area under the host coil. This suggests that the proposed system can maintain communication and WPT over a certain period, even when the host node is in motion, as in vehicle-mounted inspection applications. However, the figure also reveals that the coupling coefficient exhibits a local minimum in the lower diagonal region of the coil. This is because the magnetic field is predominantly horizontal, reducing perpendicular flux through the client coil as shown in Fig. 13. Since the communicable and powerable range depends on factors such as vehicle speed and data transmission rate, future applications will require coil design optimizations, such as geometry modifications, to enhance stability in dynamic scenarios.

B. Comparison and Analysis of Power Receiver Circuits

The proposed system uses a full-wave rectifier instead of a current chopper-based power receiver proposed in [10], as described in Section II. This is because, under the proposed system configuration, omitting current chopper control improves receiving power and cold-start capability. This section verifies this reasoning through qualitative circuit analysis.

First, we analyze the performance of current chopper-based WPT. Fig. 14 shows the circuit structure and operation of the current chopper-based WPT method proposed in [10]. The power receiver consists of a half-wave rectifier with an additional switch. Once the switch is closed, the LC tank stores energy. As soon as the current flowing through the power receiving coil reaches its peak, the switch is opened. As a result, the receiving coil tries to keep current flowing, and therefore, a sufficiently high voltage is generated at the coil to charge the storage capacitor.

Fig. 15 illustrates how current chopper control improves power transfer efficiency. The normal half-wave rectifier without a switch rectifies only the positive half-cycle of ac current in the receiver coil to charge the capacitor. Consequently, the energy of the negative half-cycle of the ac current is discarded. In a current chopper-based WPT, shorting the circuit with the switch enables the storage of energy corresponding to the negative half-cycle of the ac current in the LC tank. When the switch is opened, the stored energy in the LC tank is transferred as positive current to the capacitor. As a result, current chopper control improves power transfer efficiency by capturing and using energy from the negative half-cycle of ac current.

In contrast, the full-wave rectifier uses two diodes to rectify both the positive and negative half-cycles of ac current, extracting energy from both to charge the capacitors. Thus, whether the current chopper-based wireless power receiver [10] or the full-wave rectifier achieves higher power transfer efficiency depends on specific factors such as the current level and losses caused by diodes, which vary depending on the application. To compare the receivable power of the current chopper-based receiver [10] with that of the full-wave rectifier, we implemented the method proposed in [10] and conducted experiments under the same conditions as in Section III-C. The results showed that the current chopper-based WPT [10] achieved received power of 1.10 mW, which is lower than the 1.52 mW achieved with the full-wave rectifier. This confirms that the full-wave rectifier is more suitable for our application.

C. Comparison to State-of-the-Art

This section compares the energy consumption per bit of the proposed method with the state-of-the-art focusing on the tradeoff between communication distance and energy consumption per bit.

While the feasibility of the system was validated in Section III with discrete components, further improvements in power efficiency are expected by custom CMOS chip design. We conducted simulations using the TSMC 180-nm process to examine the relationship between the maximum achievable communication distance and the energy required to transmit a single bit. By adjusting the MOSFET gate width to modify the on-resistance, we evaluated the communicable distance for varying gate capacitances, which directly impact the energy consumption per bit. When the on-resistance of the MOSFET increases, the losses at the client node also increase, thereby reducing the communicable distance. Communication feasibility was determined by ensuring that the demodulated output exceeded 6 V. Given that the noise amplitude was 4 V, the SNR was calculated to be 3.5 dB. This relatively low SNR is attributed to the use of a preliminal prototype demodulation circuit, and improvements are expected with more advanced noise filtering designs.

Fig. 16 shows the simulation results, along with comparisons to state-of-the-art studies. As the distance becomes shorter and the coupling coefficient between coils increases, higher voltages are induced in the coil L_c. For short communication distances, where the coupling coefficient is high, the induced voltage at receiver coil may exceed the MOSFET breakdown voltage. To address this issue, configurations with

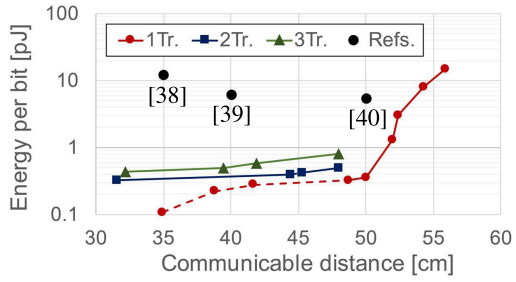

Fig. 16. Relationship between communication distance and energy per bit.

two or three vertically stacked MOSFETs were also simulated, as shown in Fig. 16. The dotted sections in the figure indicate cases where the voltage between the drain and source of the MOSFET exceeds the 5-V limit [37], suggesting that such configurations may not be feasible. It should be noted that when stacking MOSFETs vertically, a bootstrap circuit becomes necessary to maintain proper gate control. The simulation results confirm that the proposed system achieves superior energy efficiency compared with state-of-the-art methods. The communication distance with the proposed method can be extended at the cost of increased energy consumption per bit.

V. Conclusion

This article proposed a magnetic-field-based backscatter communication method that achieves ultralow-power communication by modulating the ac magnetic field for WPT. The proposed circuit enables the client node to share a single coil for both communication and power reception, contributing to device miniaturization and circuit simplification. The client node modulates the magnetic field for WPT through chopper control of the current in its power receiver coil, enabling communication without oscillators or energy storage components. The proposed method demonstrated a receivable power of 1.52 mW and a communication energy of 0.36 pJ/bit at a distance of 50 cm, outperforming state-of-the-art methods in long-range communication scenarios. These results confirm the method's potential for scalable, energy-efficient applications such as embedded sensors in RC structures.

References

[1] D. E. Bloom, D. Canning, and G. Fink, "Implications of population ageing for economic growth," *Oxford Rev. Econ. Policy*, vol. 26, no. 4, pp. 583–612, Dec. 2010.

[2] D. Acemoglu and P. Restrepo, "Demographics and automation," *Rev. Econ. Stud.*, vol. 89, no. 1, pp. 1–44, Jan. 2022.

[3] H. Takamine, K. Watabe, H. Miyata, H. Asaue, T. Nishida, and T. Shiotani, "Efficient damage inspection of deteriorated RC bridge deck with rain-induced elastic wave," *Construct. Building Mater.*, vol. 162, pp. 908–913, Feb. 2018.

[4] T. Shiotani, T. Nishida, H. Asaue, and Y. Kobayashi, "Interpretation of fatigue damage evolution in RC slabs by means of innovative 3D AE tomography," in *Proc. 9th Int. Conf. Fract. Mech. Concrete Concrete Struct.*, vol. 2, May 2016, pp. 1–12, doi: 10.21012/FC9.225. [Online]. Available: https://www.framcos.org/FraMCoS-9.php#gsc.tab=0

[5] T. S. H. Asaue, T. Nishida, T. Maeshima, and Y. Tanaka, "Evolution of fatigue damage in wheel-loading tests evaluated by 3D elastic-wave tomography," *J. Disaster Res.*, vol. 12, no. 3, pp. 487–495, Jun. 2017.

[6] T. Tanaka, R. Shirai, and M. Hashimoto, "DC magnetic field-based analytical localization robust to known stationary magnetic object," in *Proc. IEEE 65th Int. Midwest Symp. Circuits Syst. (MWSCAS)*, Aug. 2022, pp. 1–4.

[7] R. Shirai and M. Hashimoto, "DC magnetic field based 3D localization with single anchor coil," *IEEE Sensors J.*, vol. 20, no. 7, pp. 3902–3913, Apr. 2020.

[8] R. Shirai, Y. Itoh, and M. Hashimoto, "Make it trackable: An instant magnetic tracking system with coil-free tiny trackers," *IEEE Access*, vol. 9, pp. 26616–26632, 2021.

[9] A. Kurs, A. Karalis, R. Moffatt, J. D. Joannopoulos, P. Fisher, and M. Soljačić, "Wireless power transfer via strongly coupled magnetic resonances," *Science*, vol. 317, no. 5834, pp. 83–86, 2007.

[10] H. S. Gougheri and M. Kiani, "Current-based resonant power delivery with multi-cycle switching for extended-range inductive power transmission," *IEEE Trans. Circuits Syst. I, Reg. Papers*, vol. 63, no. 9, pp. 1543–1552, Sep. 2016.

[11] G. A. Covic and J. T. Boys, "Inductive power transfer," *Proc. IEEE*, vol. 101, no. 6, pp. 1276–1289, Jun. 2013.

[12] Z. Ning Low, R. A. Chinga, R. Tseng, and J. Lin, "Design and test of a high-power high-efficiency loosely coupled planar wireless power transfer system," *IEEE Trans. Ind. Electron.*, vol. 56, no. 5, pp. 1801–1812, May 2009.

[13] C. Degen, "Inductive coupling for wireless power transfer and near-field communication," *EURASIP J. Wireless Commun. Netw.*, vol. 2021, no. 1, p. 121, Dec. 2021.

[14] R. Tei, H. Yamazawa, and T. Shimizu, "BLE power consumption estimation and its applications to smart manufacturing," in *Proc. 54th Annu. Conf. Soc. Instrum. Control Engineers Jpn. (SICE)*, Jul. 2015, pp. 148–153.

[15] A. E. Boualouache, O. Nouali, S. Moussaoui, and A. Derder, "A BLE-based data collection system for IoT," in *Proc. 1st Int. Conf. New Technol. Inf. Commun. (NTIC)*, Nov. 2015, pp. 1–5.

[16] G. Loubet, A. Sidibe, A. Takacs, and D. Dragomirescu, "Battery-free Bluetooth low energy sensing nodes for structural health monitoring of concretes," in *Proc. 13th Int. Workshop Structural Health Monitor.*, 2022, pp. 1–9, doi: 10.12783/shm2021/36247.

[17] W. Hlaing, S. Thepphaeng, V. Nontaboot, N. Tangsunantham, T. Sangsuwan, and C. Pira, "Implementation of WiFi-based single phase smart meter for Internet of Things (IoT)," in *Proc. Int. Electr. Eng. Congr. (iEECON)*, Mar. 2017, pp. 1–4.

[18] H. Lakdawala et al., "A 32 nm SoC with dual core ATOM processor and RF WiFi transceiver," *IEEE J. Solid-State Circuits*, vol. 48, no. 1, pp. 91–103, Jan. 2013.

[19] M. Hernandez-Aguila, J.-L. Olvera-Cervantes, A.-E. Perez-Ramos, and A. Corona-Chavez, "WiFi sensor node with high sensitivity and linearity based on a quarter-wavelength resonator for measuring crack width," *IEEE Sensors J.*, vol. 23, no. 23, pp. 28883–28890, Dec. 2023.

[20] H.-L. Chen, S. Mardmomen, and G. Leon, "On-site measurement of heat of hydration of delivered mass concrete," *Construct. Building Mater.*, vol. 269, Oct. 2020, Art. no. 121246.

[21] J. K. Kim, K. H. Kim, and J. K. Yang, "Thermal analysis of hydration heat in concrete structures with pipe-cooling system," *Comput. Struct.*, vol. 79, no. 2, pp. 163–171, Jan. 2001.

[22] K.-B. Park, N.-Y. Jee, I.-S. Yoon, and H.-S. Lee, "Prediction of temperature distribution in high-strength concrete using hydration model," *ACI Mater. J.*, vol. 105, no. 2, p. 180, 2008.

[23] Y. Guo, G. Wang, G. Li, M. Jia, and B. Ai, "Energy efficiency gains for wireless communication systems aided by ambient backscatter," in *Proc. IEEE 93rd Veh. Technol. Conf.*, Apr. 2021, pp. 1–5.

[24] A. N. Parks, A. Liu, S. Gollakota, and J. R. Smith, "Turbocharging ambient backscatter communication," *ACM SIGCOMM Comput. Commun. Rev.*, vol. 44, no. 4, pp. 619–630, 2014.

[25] X. Lu, D. Niyato, H. Jiang, D. I. Kim, Y. Xiao, and Z. Han, "Ambient backscatter assisted wireless powered communications," *IEEE Wireless Commun.*, vol. 25, no. 2, pp. 170–177, Apr. 2018.

[26] D. Galappaththige, C. Tellambura, and A. Maaref, "Integrated sensing and backscatter communication," *IEEE Wireless Commun. Lett.*, vol. 12, no. 12, pp. 2043–2047, Dec. 2023.

[27] R. Yang, K. A. Ahmed, and M. Alioto, "Backscattered software-defined radio for flexible, reusable and upgradeable transmitters with 34–58 pJ/bit energy across common standards in 180 nm," in *Proc. IEEE Eur. Solid-State Electron. Res. Conf. (ESSERC)*, Sep. 2024, pp. 93–96.

[28] S. Kisseleff, I. F. Akyildiz, and W. H. Gerstacker, "Survey on advances in magnetic induction-based wireless underground sensor networks," *IEEE Internet Things J.*, vol. 5, no. 6, pp. 4843–4856, Dec. 2018.
[29] K. Niitsu et al., "Daisy chain transmitter for power reduction in inductive-coupling CMOS link," *IEICE Trans. Electron.*, vol. 90, no. 4, pp. 829–835, Apr. 2007.
[30] A. Wibisono, M. H. Alsharif, H. Song, and B. M. Lee, "A survey on underwater wireless power and data transfer system," *IEEE Access*, vol. 12, pp. 34942–34957, 2024.
[31] H. Guo, Z. Sun, and P. Wang, "Multiple frequency band channel modeling and analysis for magnetic induction communication in practical underwater environments," *IEEE Trans. Veh. Technol.*, vol. 66, no. 8, pp. 6619–6632, Aug. 2017.
[32] Y. Liu, Y. Yao, and W.-H. Ki, "A 13.56-MHz single-input dual-output wireless power and data transfer system for bio-implants," *IEEE J. Solid-State Circuits*, vol. 59, no. 8, pp. 2557–2567, Aug. 2024.
[33] N. Miura, D. Mizoguchi, T. Sakurai, and T. Kuroda, "Analysis and design of inductive coupling and transceiver circuit for inductive inter-chip wireless superconnect," *IEEE J. Solid-State Circuits*, vol. 40, no. 4, pp. 829–837, Apr. 2005.
[34] D. Guermandi, S. Gambini, and J. Rabaey, "A 1 V 250 KPPS 90 NM CMOS pulse based transceiver for CM-range wireless communication," in *Proc. 33rd Eur. Solid-State Circuits Conf.*, Sep. 2007, pp. 135–138.
[35] R. Zhao et al., "NFC+: Breaking NFC networking limits through resonance engineering," in *Proc. Annu. Conf. ACM Special Interest Group Data Commun. Appl., Technol., Architectures, Protocols Comput. Commun.*, Jul. 2020, pp. 694–707.
[36] A. Pal and K. Kant, "NFMI: Near field magnetic induction based communication," *Comput. Netw.*, vol. 181, Nov. 2020, Art. no. 107548.
[37] R. Barsatan, T. Y. Man, and M. Chan, "A CMOS-compatible WORM memory for low-cost non-volatile memory applications," in *Proc. IEEE Conf. Electron Devices Solid-State Circuits*, Jan. 2005, pp. 339–342.
[38] J. Rosenthal, A. Sharma, E. Kampianakis, and M. S. Reynolds, "A 25 Mbps, 12.4 pJ/b DQPSK backscatter data uplink for the NeuroDisc brain–computer interface," *IEEE Trans. Biomed. Circuits Syst.*, vol. 13, no. 5, pp. 858–867, Oct. 2019.
[39] H. Afzal, C. Li, and O. Momeni, "A highly efficient 165-GHz 4FSK 17-Gb/s transceiver system with frequency overlapping architecture in 65-nm CMOS," *IEEE J. Solid-State Circuits*, vol. 58, no. 11, pp. 3113–3126, Nov. 2023.
[40] S.-K. Kuo, M. Dunna, H. Lu, A. Agarwal, D. Bharadia, and P. P. Mercier, "LTE-powered BLE-to-WiFi backscattering chip toward single-device interrogation RFID-like systems," *IEEE Solid-State Circuits Lett.*, vol. 6, pp. 225–228, 2023.

Ryota Fukugasako received the B.E. degree in engineering and the M.S. degree in informatics from Kyoto University, Kyoto, Japan, in 2023 and 2025, respectively.

His research interests include inductive wireless power transfer and inductive wireless communication.

Hisafumi Asaue received the B.E., M.E., and Ph.D. degrees in civil engineering from Kumamoto University, Kumamoto, Japan, in 2000, 2002, and 2005, respectively.

He is currently an Associate Professor at the Innovative Technology on Infrastructure Laboratory (ITIL), Kyoto University, Kyoto, Japan. His current research interests include efficient maintenance of civil engineering structures through the application of sensing technology and the development of advanced nondestructive testing technologies.

Dr. Asaue was a recipient of the Structural Faults and Repair NDT Award from Engineering Technics Press, Edinburgh, Scotland, in 2016, and the SGEPSS Outstanding Paper Award from the Society of Geomagnetism and Earth, Planetary and Space Science in 2022.

Tomoki Shiotani is a Professor at the Innovative Technology on Infrastructure Laboratory (ITIL) and the Deputy Leader of the Consortium of Innovative Technology for Infrastructures, Kyoto University, Kyoto, Japan. After working as a General Contractor and a Senior Research Fellow at Delft University of Technology, Delft, The Netherlands. He joined Kyoto University, as an Associate Professor, in 2007. In 2014, he became a Professor, leading research in innovative technologies for infrastructure. He has published more than 200 peer-reviewed papers and holds more than 60 patents. His research focuses on advanced nondestructive testing (NDT) methods for assessing infrastructure such as road bridges, dams, and tunnels.

Dr. Shiotani chaired RILEM TC-269IAM, which concluded in 2023, and currently leads a new committee on the assessment of 3-D-printed concrete (3DPC) using NDT, starting in 2024. His numerous accolades are four NDT awards from the Structural Faults and Repair Conference (U.K.) in 2008, 2013, 2016, and 2018, as well as prestigious honors from the AEWG (USA), including the Fellow Award in 2013, the Joseph Kaiser Achievement Award in 2017, and the Gold Medal in 2019, its highest distinction. In 2021, he was recognized among the top 2% of scientists in the world by Stanford University. He currently serves as the President for the International Institute of Innovative Acoustic Emission (IIIAE), representing major AE groups in USA, Japan, and Europe.

Masanori Hashimoto (Senior Member, IEEE) received the B.E., M.E., and Ph.D. degrees in communications and computer engineering from Kyoto University, Kyoto, Japan, in 1997, 1999, and 2001, respectively.

He is currently a Professor with the Graduate School of Informatics, Kyoto University. His research interests include VLSI design for reliability, timing and power integrity analysis, reconfigurable computing, soft error characterization, and low-power circuit design.

Dr. Hashimoto was the TPC Chair of Asia and South Pacific Design Automation Conference (ASP-DAC) in 2022 and the International Midwest Symposium on Circuits and Systems (MWSCAS) in 2022. He was/is on the Technical Program Committees of international conferences, including the Design Automation Conference (DAC), the International Conference on Computer-Aided Design (ICCAD), the International Test Conference (ITC), the Symposium on VLSI Circuits, and the Design, Automation and Test in Europe Conference (DATE). He serves/served as the Editor-in-Chief for *Microelectronics Reliability* (Elsevier) and an Associate Editor for IEEE TRANSACTIONS ON VERY LARGE SCALE INTEGRATION SYSTEMS (VLSI), IEEE TRANSACTIONS ON CIRCUITS AND SYSTEMS—I: REGULAR PAPERS, and *ACM Transactions on Design Automation of Electronic Systems* (TODAES).

Ryo Shirai (Member, IEEE) received the B.E., M.E., and Ph.D. degrees in information systems engineering from Osaka University, Suita, Japan, in 2016, 2018, and 2021, respectively.

He is currently an Assistant Professor with the Graduate School of Informatics, Kyoto University, Kyoto, Japan. His current research interests include analog circuit design, embedded systems, and sensor systems.

Dr. Shirai is a member of the Institute of Electronics, Information and Communication Engineers (IEICE).